

Theoretical aspects of the smoothed finite element method (SFEM)

G. R. Liu^{1,2,*}, T. T. Nguyen¹, K. Y. Dai^{1,2} and K. Y. Lam³

¹*Center for Advanced Computations in Engineering Science (ACES), Department of Mechanical Engineering, National University of Singapore, 9 Engineering Drive 1, Singapore 117576, Singapore*

²*Singapore-MIT Alliance (SMA), E4-04-10, 4 Engineering Drive 3, Singapore 117576, Singapore*

³*School of Mechanical and Aerospace Engineering, Nanyang Technological University, 50 Nanyang Avenue, Singapore 639798, Singapore*

SUMMARY

This paper examines the theoretical bases for the smoothed finite element method (SFEM), which was formulated by incorporating cell-wise strain smoothing operation into standard compatible finite element method (FEM). The weak form of SFEM can be derived from the Hu–Washizu three-field variational principle. For elastic problems, it is proved that 1D linear element and 2D linear triangle element in SFEM are identical to their counterparts in FEM, while 2D bilinear quadrilateral elements in SFEM are different from that of FEM: when the number of smoothing cells (SCs) of the elements equals 1, the SFEM solution is proved to be ‘variationally consistent’ and has the same properties with those of FEM using reduced integration; when SC approaches infinity, the SFEM solution will approach the solution of the standard displacement compatible FEM model; when SC is a finite number larger than 1, the SFEM solutions are not ‘variationally consistent’ but ‘energy consistent’, and will change monotonously from the solution of SFEM (SC = 1) to that of SFEM (SC → ∞). It is suggested that there exists an optimal number of SC such that the SFEM solution is closest to the exact solution. The properties of SFEM are confirmed by numerical examples. Copyright © 2006 John Wiley & Sons, Ltd.

Received 2 May 2006; Revised 25 September 2006; Accepted 15 November 2006

KEY WORDS: finite element method (FEM); smoothed finite element method (SFEM); strain smoothing; reduced integration; compatible model; assumed strain method

1. INTRODUCTION

For several decades, many useful numerical methods have been proposed to develop lower-order finite elements with good performance in solving practical problems, especially, for enhanced accuracy in coarse meshes and free of spurious locking. Although there are some exceptions, most

*Correspondence to: G. R. Liu, Center for Advanced Computations in Engineering Science (ACES), Department of Mechanical Engineering, National University of Singapore, 9 Engineering Drive 1, Singapore 117576, Singapore.

†E-mail: mpeliugr@nus.edu.sg

of them can be grouped into the equilibrium models based on the complementary energy principle, the displacement models based on the potential energy principle [1] and the mixed models which in addition to displacements, assume one or more independent fields such as stresses or strains [2], such as the assumed strain method proposed by Simo and Hughes [3] based on the Hu–Washizu principle [4]. The key point of the method lies in the strain field in which the standard discrete gradient operator is replaced by an assumed gradient operator. One of the assumed strain methods is the smoothed strain method, proposed by Chen *et al.* [5], in the context of mesh-free method. The aim of this method is to stabilize the nodal integration for a Galerkin mesh-free method by using a strain smoothing technique. The method shows higher efficiency, desired accuracy and convergent properties. Yoo *et al.* then extended the stabilized nodal integration to the natural-element method and solved the nearly incompressible problems without any modification of integration scheme [6]. Liu *et al.* introduced the nodal integration into the point interpolation method and the radial point interpolation method to install linear conformability and good performance has been observed for many problems including contact problems [7].

So far, displacement finite element method (FEM) models have been used most popularly for engineering problems. However, it is well known that FEM produces the overestimation of stiffness matrix, and the model is in general too stiff with the internal strain energy being underestimated [1]. The consequence is that the solution is always smaller than the real solution. In addition, because mapping and co-ordinate transformation is involved in the FEM, its element is not allowed to be of arbitrary shape. A necessary condition for a 4-node isoparametric element is that no interior angle is greater than 180° and the positivity of Jacobian determinant should be ensured in numerical implementation [8–10]. This not only increases the computational cost but also limits the ability of the application of FEM to the large deformation problems with severe element distortion. In the effort of overcoming these problems of FEM, Liu *et al.* proposed for the first time a smoothed finite element method (SFEM) by combining the existing FEM technology and the strain smoothing technique of mesh-free methods [11]. In this method, elements are used as in the FEM, and smoothing operations are performed over the elements. Depending on the requirement of accuracy and stability, an element may be further subdivided into several smoothing cells (SCs), and the smoothing operation is then performed for each SC within an element. Galerkin weak form is used as in FEM, but smoothed strains are used for computing the stiffness matrix. When choosing a constant smoothing function, area integrations over the cell in the weak form become line integrations along the cell boundaries. Hence, no derivative of shape functions is involved in computing the field gradients to form the stiffness matrix. Numerical studies have demonstrated that SFEM shows some superiorities over the standard FEM using 4-node isoparametric elements. For examples, (1) SFEM gives better results than that of FEM in both displacement and energy because the stiffness of SFEM is softer than that of FEM; (2) domain discretization of SFEM is more flexible than FEM when the severe distorted, tile and polygonal elements can be used; (3) field gradients are computed directly using only shape functions itself; (4) construction of shape functions can be much easier than that in the FEM, which practically allows explicit interpolations of field variables; and (5) many existing algorithms of FEM can be modified easily and applied to SFEM. Most importantly, these good features are gained without increasing the efforts both in modelling and computation, and the changes to the existing FEM code are also very minimum. All these features have been demonstrated in detail by Liu *et al.* using many numerical examples and elements of complex shapes including extremely distorted quadrilateral elements, polygon and tile elements [11]. However, the theoretical bases of SFEM are still not very clear, the related theory has not been set

up and properly proved, and rigorous formulations have not been given out and examined in detail.

This paper aims to establish the theoretical foundations for SFEM. The weak form will be obtained based on the Hu–Washizu three-field variational principle. The properties of SFEM will be examined. All these theoretical findings will be confirmed with numerical tests.

The paper is outlined as follows. In Section 2, the idea of SFEM is briefly introduced. In Section 3, variational principle for SFEM is described. The properties of the single-cell bilinear quadrilateral smoothed finite element are analysed in Section 4. In Section 5, variational consistency of SFEM is examined. Section 6 presents numerical examples to verify the formulations and properties of the SFEM. Some concluding remarks are made in the Section 7.

2. BRIEFING ON THE SMOOTHED FINITE ELEMENT METHOD (SFEM)

2.1. Basic equations for elasticity [9]

Consider a 2D static elasticity problem governed by equilibrium equations defined in the domain Ω bounded by Γ and $\Gamma = \Gamma_u \cup \Gamma_t$, $\Gamma_u \cap \Gamma_t = \emptyset$

$$\nabla_S^T \boldsymbol{\sigma} + \mathbf{b} = \mathbf{0} \quad \text{in } \Omega \quad (1)$$

where $\mathbf{0}$ is a null vector, $\boldsymbol{\sigma}$ is the stress tensor written in vector form

$$\boldsymbol{\sigma}^T = \{\sigma_{xx} \quad \sigma_{yy} \quad \sigma_{xy}\} \quad (2)$$

\mathbf{b} is the vector of external body forces in the x - and y -direction

$$\mathbf{b} = \begin{Bmatrix} b_x \\ b_y \end{Bmatrix} \quad (3)$$

and ∇_S is a differential operator matrix given by

$$\nabla_S = \begin{bmatrix} \frac{\partial}{\partial x} & 0 \\ 0 & \frac{\partial}{\partial y} \\ \frac{\partial}{\partial y} & \frac{\partial}{\partial x} \end{bmatrix} \quad (4)$$

Boundary conditions are given as follows:

$$\mathbf{u} = \bar{\mathbf{u}} \quad \text{on } \Gamma_u \quad (5)$$

$$\mathbf{n}^T \boldsymbol{\sigma} = \bar{\mathbf{t}} \quad \text{on } \Gamma_t \quad (6)$$

where $\bar{\mathbf{u}} = \{\bar{u}_x \quad \bar{u}_y\}^T$ is the prescribed displacement vector on the essential boundary Γ_u ; $\bar{\mathbf{t}} = \{\bar{t}_x \quad \bar{t}_y\}^T$ is the prescribed traction vector on the natural boundary Γ_t ; \mathbf{n} is the unit outward normal matrix

given by

$$\mathbf{n} = \begin{bmatrix} n_x & 0 \\ 0 & n_y \\ n_y & n_x \end{bmatrix} \quad (7)$$

and \mathbf{u} is the displacement vector of the form

$$\mathbf{u} = \begin{Bmatrix} u \\ v \end{Bmatrix} \quad (8)$$

where u, v are the displacement components in the x - and y -direction, respectively.

The strain–displacement relation or the compatibility equation is given by

$$\boldsymbol{\varepsilon} = \nabla_S \mathbf{u} \quad (9)$$

where $\boldsymbol{\varepsilon}$ is the strain tensor written in vector form

$$\boldsymbol{\varepsilon}^T = \{\varepsilon_{xx} \quad \varepsilon_{yy} \quad \gamma_{xy}\} \quad (10)$$

The stress–strain relation or the Hooke's law is

$$\boldsymbol{\sigma} = \mathbf{D}\boldsymbol{\varepsilon} \quad (11)$$

where \mathbf{D} is a symmetric positive definite (SPD) matrix of material constants.

2.2. The finite element method (FEM) (see, e.g. References [8–10])

The discrete equations are generated from the Galerkin weak form

$$\int_{\Omega} (\nabla_S \delta \mathbf{u})^T \mathbf{D} (\nabla_S \mathbf{u}) \, d\Omega - \int_{\Omega} (\delta \mathbf{u})^T \mathbf{b} \, d\Omega - \int_{\Gamma_t} (\delta \mathbf{u})^T \bar{\mathbf{t}} \, d\Gamma = 0 \quad (12)$$

where $\mathbf{u} \in H^1(\Omega)$ are trial functions and $\delta \mathbf{u} \in H_0^1(\Omega)$ are test functions. Here, $H^1(\Omega)$ denotes the Sobolev space of functions with square integrable derivatives in Ω , and $H_0^1(\Omega)$ is the subset of $H^1(\Omega)$ with vanishing values on Γ_u [2]. The FEM uses the following trial and test functions:

$$\mathbf{u}^h(\mathbf{x}) = \sum_{I=1}^{\text{NP}} \mathbf{N}_I(\mathbf{x}) \mathbf{d}_I, \quad \delta \mathbf{u}^h(\mathbf{x}) = \sum_{I=1}^{\text{NP}} \mathbf{N}_I(\mathbf{x}) \delta \mathbf{d}_I \quad (13)$$

where NP is the number of the nodal variables of the element, $\mathbf{d}_I = [u_I \ v_I]^T$ is the nodal displacement vector and

$$\mathbf{N}_I(\mathbf{x}) = \begin{bmatrix} N_I(\mathbf{x}) & 0 \\ 0 & N_I(\mathbf{x}) \end{bmatrix}$$

is the shape function matrix which satisfies the conditions

$$N_I(\mathbf{x}_J) = \delta_{IJ} \quad \text{and} \quad \sum_{I=1}^{\text{NP}} N_I(\mathbf{x}) = 1 \quad (14)$$

where δ_{IJ} is the Kronecker delta.

By substituting the approximations, \mathbf{u}^h and $\delta\mathbf{u}^h$, into the weak form and invoking the arbitrariness of virtual nodal displacements, Equation (12) yields the standard discretized algebraic system equation:

$$\mathbf{K}^{\text{FEM}}\mathbf{d} = \mathbf{f} \quad (15)$$

where \mathbf{K}^{FEM} is the stiffness matrix, \mathbf{f} is the element force vector, with entries of

$$\mathbf{K}_{IJ}^{\text{FEM}} = \int_{\Omega} \mathbf{B}_I^T \mathbf{D} \mathbf{B}_J \, d\Omega \quad (16)$$

$$\mathbf{f}_I = \int_{\Omega} \mathbf{N}_I^T(\mathbf{x}) \mathbf{b} \, d\Omega + \int_{\Gamma_I} \mathbf{N}_I^T(\mathbf{x}) \bar{\mathbf{t}} \, d\Gamma \quad (17)$$

with the *strain matrix* defined as

$$\mathbf{B}_I(\mathbf{x}) = \nabla_S N_I(\mathbf{x}) = \begin{bmatrix} \frac{\partial N_I(\mathbf{x})}{\partial x} & 0 \\ 0 & \frac{\partial N_I(\mathbf{x})}{\partial y} \\ \frac{\partial N_I(\mathbf{x})}{\partial y} & \frac{\partial N_I(\mathbf{x})}{\partial x} \end{bmatrix} \quad (18)$$

2.3. The smoothed finite element method (SFEM) [11]

The SFEM combines the existing FEM procedure with a strain smoothing operation. In the SFEM method, elements are used as in the FEM, and smoothing operations are performed over the SCs. The final discretized algebraic system equation has the form

$$\mathbf{K}^{\text{SFEM}}\mathbf{d} = \mathbf{f} \quad (19)$$

where \mathbf{K}^{SFEM} is the *smoothed* stiffness matrix given by

$$\mathbf{K}_{IJ}^{\text{SFEM}} = \sum_{C=1}^{\text{SC}} \int_{\Omega_C} \tilde{\mathbf{B}}_{CI}^T \mathbf{D} \tilde{\mathbf{B}}_{CJ} \, d\Omega = \sum_{C=1}^{\text{SC}} \tilde{\mathbf{B}}_{CI}^T \mathbf{D} \tilde{\mathbf{B}}_{CJ} A_C \quad (20)$$

where $A_C = \int_{\Omega_C} d\Omega$ is the area of domain Ω_C , SC is the number of SCs that divides from the domain Ω such that $\Omega = \Omega_1 \cup \Omega_2 \cup \dots \cup \Omega_{\text{SC}}$ and $\Omega_1 \cap \Omega_2 \cap \dots \cap \Omega_{\text{SC}} = \emptyset$, and $\tilde{\mathbf{B}}_{CI}$ is the *smoothed* strain matrix which is obtained by the following strain smoothing operation:

$$\tilde{\boldsymbol{\varepsilon}}_C^h = \int_{\Omega_C} \boldsymbol{\varepsilon}^h(\mathbf{x}) \Phi_C(\mathbf{x}) \, d\Omega \quad (21)$$

where $\boldsymbol{\varepsilon}^h(\mathbf{x}) = \nabla_S \mathbf{u}^h(\mathbf{x})$ is the strain obtained from displacement with compatibility, $\Phi_C(\mathbf{x})$ is a given smoothing function that satisfies at least unity property

$$\int_{\Omega_C} \Phi_C(\mathbf{x}) \, d\Omega = 1 \quad (22)$$

Using the following constant smoothing function

$$\Phi_C(\mathbf{x}) = \begin{cases} 1/A_C, & \mathbf{x} \in \Omega_C \\ 0, & \mathbf{x} \notin \Omega_C \end{cases} \quad (23)$$

and applying a divergence theorem, one can get the smoothed strain of the domain Ω_C

$$\begin{aligned} \tilde{\boldsymbol{\varepsilon}}_C^h &= \int_{\Omega_C} \nabla_S \mathbf{u}^h(\mathbf{x}) \frac{1}{A_C} d\Omega = \frac{1}{A_C} \int_{\Omega_C} \nabla_S \mathbf{u}^h(\mathbf{x}) d\Omega \\ &= \frac{1}{A_C} \int_{\Gamma_C} \mathbf{n}_C(\mathbf{x}) \mathbf{u}^h(\mathbf{x}) d\Gamma \end{aligned} \quad (24)$$

where Γ_C is the boundary of the domain Ω_C , and $\mathbf{n}_C(\mathbf{x})$ is the outward normal vector matrix on the boundary Γ_C and has the form similarly to Equation (7).

Substituting Equation (13) into Equation (24), one obtains the smoothed strain as

$$\tilde{\boldsymbol{\varepsilon}}_C^h = \sum_{I=1}^{NP} \tilde{\mathbf{B}}_{CI} \mathbf{d}_I \quad (25)$$

where the smoothed strain matrix $\tilde{\mathbf{B}}_{CI}$ is calculated by

$$\tilde{\mathbf{B}}_{CI} = \frac{1}{A_C} \int_{\Gamma_C} N_I(\mathbf{x}) \mathbf{n}_C(\mathbf{x}) d\Gamma = \begin{bmatrix} \frac{1}{A_C} \int_{\Gamma_C} N_I(\mathbf{x}) n_{Cx}(\mathbf{x}) d\Gamma & 0 \\ 0 & \frac{1}{A_C} \int_{\Gamma_C} N_I(\mathbf{x}) n_{Cy}(\mathbf{x}) d\Gamma \\ \frac{1}{A_C} \int_{\Gamma_C} N_I(\mathbf{x}) n_{Cy}(\mathbf{x}) d\Gamma & \frac{1}{A_C} \int_{\Gamma_C} N_I(\mathbf{x}) n_{Cx}(\mathbf{x}) d\Gamma \end{bmatrix} \quad (26)$$

It is easy to reveal the relation between the smoothed strain matrix $\tilde{\mathbf{B}}_{CI}$ with the standard strain matrix of FEM $\mathbf{B}_I(\mathbf{x}) = \nabla_S N_I(\mathbf{x})$ through the following equation:

$$\begin{aligned} \tilde{\mathbf{B}}_{CI} &= \int_{\Gamma_C} \frac{1}{A_C} N_I(\mathbf{x}) \mathbf{n}_C(\mathbf{x}) d\Gamma = \int_{\Omega_C} \frac{1}{A_C} \nabla_S N_I(\mathbf{x}) d\Omega \\ &= \frac{1}{A_C} \int_{\Omega_C} \mathbf{B}_I(\mathbf{x}) d\Omega \end{aligned} \quad (27)$$

Equation (27) states that the smoothed strain matrix $\tilde{\mathbf{B}}_{CI}$ is the average value of the standard strain matrix $\mathbf{B}_I(\mathbf{x})$ over the smoothing domain Ω_C .

Note that the SFEM allows us to create a sequence of SFEM model by using different number of SCs. We will reveal and prove the bound properties of the sequence of SFEM models in the following sections.

Lemma 1

The assumed strains using strain smoothing defined in Equation (21) ensure a stress equilibrium state within the cell that is free of body force.

Proof

Using Equation (21), the assumed strains become constants at any point in the cell. The stresses obtained using Equation (11) are therefore also constants in the cell. These constant stresses satisfy naturally the equilibrium equation (1) when $\mathbf{b} = \mathbf{0}$. \square

Lemma 1 is an extremely powerful statement: application of strain smoothing to a cell in the problem domain results in a stress equilibrium in the cell. We, therefore, call the smoothing operation a *stress equilibrator*.

Lemma 2

The assumed strains, using Equation (21), will not be compatible with an assumed displacement field that is higher than (strictly) first order.

Proof

If the order of the displacement field is higher than first order, the strain produced by Equation (9) will not be constant. The assumed strains are, however, constants. Hence the compatibility condition is violated. \square

Lemma 2 implies that the stress equilibrator will destroy the compatibility in the cells with assumed displacement fields of bilinear or higher order.

3. VARIATIONAL PRINCIPLE FOR SFEM

In this section, the Galerkin weak form for SFEM is established from the Hu–Washizu three-field variational principle [12]:

$$\begin{aligned}
 U(\mathbf{u}, \tilde{\boldsymbol{\varepsilon}}, \boldsymbol{\sigma}) = & \int_{\Omega} \frac{1}{2} \tilde{\boldsymbol{\varepsilon}}^T \mathbf{D} \tilde{\boldsymbol{\varepsilon}} \, d\Omega - \int_{\Omega} \boldsymbol{\sigma}^T \tilde{\boldsymbol{\varepsilon}} \, d\Omega + \int_{\Omega} \boldsymbol{\sigma}^T (\nabla_S \mathbf{u}) \, d\Omega \\
 & - \int_{\Omega} \mathbf{u}^T \mathbf{b} \, d\Omega - \int_{\Gamma_t} \mathbf{u}^T \bar{\mathbf{t}} \, d\Gamma - \int_{\Gamma_u} (\mathbf{u} - \bar{\mathbf{u}})^T (\mathbf{n}^T \boldsymbol{\sigma}) \, d\Gamma
 \end{aligned} \quad (28)$$

where $\tilde{\boldsymbol{\varepsilon}}$ is the assumed strain vector.

If stresses $\boldsymbol{\sigma}$ are expressed in term of strains $\tilde{\boldsymbol{\varepsilon}}$ through the stress–strain relation $\boldsymbol{\sigma} = \mathbf{D} \tilde{\boldsymbol{\varepsilon}}$ and $\mathbf{u} = \bar{\mathbf{u}}$ on the essential boundary Γ_u , we will obtain a two-field variational principle $U(\mathbf{u}, \tilde{\boldsymbol{\varepsilon}})$. It is the modified Hellinger–Reissner variational principle with strains $\tilde{\boldsymbol{\varepsilon}}$ and displacements \mathbf{u} as independent field variables [12]:

$$U(\mathbf{u}, \tilde{\boldsymbol{\varepsilon}}) = - \int_{\Omega} \frac{1}{2} \tilde{\boldsymbol{\varepsilon}}^T \mathbf{D} \tilde{\boldsymbol{\varepsilon}} \, d\Omega + \int_{\Omega} (\mathbf{D} \tilde{\boldsymbol{\varepsilon}})^T (\nabla_S \mathbf{u}) \, d\Omega - \int_{\Omega} \mathbf{u}^T \mathbf{b} \, d\Omega - \int_{\Gamma_t} \mathbf{u}^T \bar{\mathbf{t}} \, d\Gamma \quad (29)$$

Performing the variation using the chain rule, one obtains

$$\begin{aligned} \delta U(\mathbf{u}, \tilde{\boldsymbol{\varepsilon}}) = & - \int_{\Omega} \delta \tilde{\boldsymbol{\varepsilon}}^T \mathbf{D} \tilde{\boldsymbol{\varepsilon}} \, d\Omega + \int_{\Omega} \delta \tilde{\boldsymbol{\varepsilon}}^T \mathbf{D} (\nabla_S \mathbf{u}) \, d\Omega + \int_{\Omega} \tilde{\boldsymbol{\varepsilon}}^T \mathbf{D} (\nabla_S \delta \mathbf{u}) \, d\Omega \\ & - \int_{\Omega} \delta \mathbf{u}^T \mathbf{b} \, d\Omega - \int_{\Gamma_t} \delta \mathbf{u}^T \bar{\mathbf{t}} \, d\Gamma = 0 \end{aligned} \quad (30)$$

Substituting approximations (13), (25) into (30) and using the arbitrary property of variation, we obtain

$$\mathbf{K}^{\text{two-field}} \mathbf{d} = \mathbf{f} \quad (31)$$

where $\mathbf{K}^{\text{two-field}}$ is the *smoothed* stiffness matrix, and \mathbf{f} is the element force vector given by

$$\mathbf{K}_{IJ}^{\text{two-field}} = - \int_{\Omega} \tilde{\mathbf{B}}_I^T \mathbf{D} \tilde{\mathbf{B}}_J \, d\Omega + 2 \int_{\Omega} \tilde{\mathbf{B}}_I^T \mathbf{D} \mathbf{B}_J(\mathbf{x}) \, d\Omega \quad (32)$$

$$\mathbf{f}_I = \int_{\Omega} \mathbf{N}_I^T(\mathbf{x}) \mathbf{b} \, d\Omega + \int_{\Gamma_t} \mathbf{N}_I^T(\mathbf{x}) \bar{\mathbf{t}} \, d\Gamma \quad (33)$$

When the orthogonal condition

$$\int_{\Omega} \tilde{\mathbf{B}}_I^T \mathbf{D} \mathbf{B}_J(\mathbf{x}) \, d\Omega = \int_{\Omega} \tilde{\mathbf{B}}_I^T \mathbf{D} \tilde{\mathbf{B}}_J \, d\Omega \quad (34)$$

is satisfied [4], from Equation (32) we have

$$\mathbf{K}_{IJ}^{\text{two-field}} = \int_{\Omega} \tilde{\mathbf{B}}_I^T \mathbf{D} \tilde{\mathbf{B}}_J \, d\Omega \quad (35)$$

and the mixed model is variationally consistent, and the mixed variational principle is the assumed strain method by Simo and Hughes [3]:

$$\delta U(\mathbf{u}, \tilde{\boldsymbol{\varepsilon}}) = \int_{\Omega} \delta \tilde{\boldsymbol{\varepsilon}}^T \mathbf{D} \tilde{\boldsymbol{\varepsilon}} \, d\Omega - \int_{\Omega} \delta \mathbf{u}^T \mathbf{b} \, d\Omega - \int_{\Gamma_t} \delta \mathbf{u}^T \bar{\mathbf{t}} \, d\Gamma = 0 \quad (36)$$

This is a generalized Galerkin weak form.

The SFEM uses the generalized Galerkin weak form given in Equation (36), but with the following two key assumptions:

- (1) The domain Ω is divided into a number of SCs.
- (2) The stiffness matrix is defined as Equation (20), regardless whether or not the orthogonal conditions (34) are satisfied.

Due to these two assumptions, the SFEM may or may not be ‘variationally consistent’ based on the definition of Equation (34).

Theorem 1

When linear shape functions are used, no matter how many smoothed cells Ω_C are used in Ω , the SFEM and FEM are equivalent, $\mathbf{K}_{IJ}^{\text{SFEM}} = \mathbf{K}_{IJ}^{\text{FEM}}$, and variationally consistent.

Proof

For linear shape functions, we have $\mathbf{B}_I(\mathbf{x}) = \nabla_S N_I(\mathbf{x}) = \mathbf{B}_I$ where the components of \mathbf{B}_I are constants. If we divide the domain Ω into SCs such as $\Omega = \Omega_1 \cup \Omega_2 \cup \dots \cup \Omega_{SC}$ and $\Omega_1 \cap \Omega_2 \cap \dots \cap \Omega_{SC} = \emptyset$, and use Equation (26) to calculate the smoothed strain matrix, we obtain

$$\tilde{\mathbf{B}}_{CI} = \int_{\Omega_C} \frac{\mathbf{B}_I}{A_C} d\Omega = \mathbf{B}_I \int_{\Omega_C} \frac{1}{A_C} d\Omega = \mathbf{B}_I \quad (37)$$

which gives the simple fact that the smoothed gradient matrix $\tilde{\mathbf{B}}_{CI}$ over C th cell is also the constant gradient matrix \mathbf{B}_I .

From Equations (20) and (37), the stiffness matrix of the element is calculated

$$\begin{aligned} \mathbf{K}_{IJ}^{\text{SFEM}} &= \sum_{C=1}^{\text{SC}} \int_{\Omega_C} \tilde{\mathbf{B}}_{CI}^T \mathbf{D} \tilde{\mathbf{B}}_{CJ} d\Omega = \sum_{C=1}^{\text{SC}} \int_{\Omega_C} \mathbf{B}_I^T \mathbf{D} \mathbf{B}_J d\Omega \\ &= \mathbf{B}_I^T \mathbf{D} \mathbf{B}_J \sum_{C=1}^{\text{SC}} \int_{\Omega_C} d\Omega = \mathbf{B}_I^T \mathbf{D} \mathbf{B}_J \int_{\Omega} d\Omega = \int_{\Omega} \mathbf{B}_I^T \mathbf{D} \mathbf{B}_J d\Omega \\ &= \mathbf{K}_{IJ}^{\text{FEM}} \end{aligned} \quad (38)$$

Because the solution of FEM is variationally consistent, the solution of SFEM in this case is also variationally consistent. \square

Therefore, for 1D-problem and 2D-problem using triangle elements, if linear shape functions are adopted such that $\nabla_S N_I(\mathbf{x}) = \text{const}$, the solutions of SFEM and FEM are identical irrespective of the number of smoothed cells Ω_C used in Ω . For the bilinear quadrilateral element, $\nabla_S N_I(\mathbf{x})$ is a linear function of co-ordinates (not constant), hence $\tilde{\mathbf{B}}_I \neq \mathbf{B}_I(\mathbf{x})$ and $\mathbf{K}_{IJ}^{\text{SFEM}} \neq \mathbf{K}_{IJ}^{\text{FEM}}$. Hence, the solution of SFEM will be different from that of FEM. We will study the properties of the solution of the single-cell bilinear quadrilateral smoothed finite element in next section.

4. THE PROPERTIES OF THE SINGLE-CELL BILINEAR QUADRILATERAL SMOOTHED FINITE ELEMENT

Theorem 2

If only one single-strain smoothing cell ($\text{SC} = 1$) is used individually for each element in the problem domain of a solid, the SFEM is variationally consistent.

Proof

In this case, $\Omega_C = \Omega$. From Equation (32), using constant matrices $\tilde{\mathbf{B}}_I$ and \mathbf{D} , and $A = \int_{\Omega} d\Omega$ being the area of the domain Ω , one obtains

$$\begin{aligned} \int_{\Omega} \tilde{\mathbf{B}}_I^T \mathbf{D} \mathbf{B}_J(\mathbf{x}) d\Omega &= \tilde{\mathbf{B}}_I^T \mathbf{D} \int_{\Omega} \mathbf{B}_J(\mathbf{x}) d\Omega = \tilde{\mathbf{B}}_I^T \mathbf{D} A \int_{\Omega} \frac{\mathbf{B}_J(\mathbf{x})}{A} d\Omega = \tilde{\mathbf{B}}_I^T \mathbf{D} A \tilde{\mathbf{B}}_J \\ &= \int_{\Omega} \tilde{\mathbf{B}}_I^T \mathbf{D} \tilde{\mathbf{B}}_J d\Omega \end{aligned} \quad (39)$$

which satisfies the orthogonal condition (34), and hence the SFEM is ‘variationally consistent’ by the definition of Equation (34). \square

Lemma 3

If only one single-strain smoothing cell (SC = 1) is used individually for each element in the problem domain of a solid, the solution of SFEM has the same properties with that of FEM using reduced integration (one Gauss point).

Proof

As shown in Equation (27), the smoothed strain matrix $\tilde{\mathbf{B}}_I$ of SFEM is the average value of the standard strain matrix $\mathbf{B}_I(\mathbf{x})$ over the smoothing domain Ω , the real physical domain. While for FEM using reduced integration, $\mathbf{B}_I(\mathbf{x})$ is calculated at the centre of the isoparametric element, $\xi = \eta = 0$. So $\mathbf{B}_I(\xi = 0, \eta = 0)$ in FEM is also considered to be the average value of $\mathbf{B}_I(\mathbf{x})$ over the isoparametric element. Therefore, it is clear that $\int_{\Omega} \tilde{\mathbf{B}}_I^T \mathbf{D} \tilde{\mathbf{B}}_I d\Omega$ in SFEM has the same meaning with $\int_{-1}^1 \int_{-1}^1 \mathbf{B}_I^T \mathbf{D} \mathbf{B}_I \mathbf{J} d\xi d\eta$ in FEM using reduced integration. The only difference is that $\mathbf{B}_I(\xi = 0, \eta = 0)$ in FEM is the average value of $\mathbf{B}_I(\mathbf{x})$ over the isoparametric element and $\tilde{\mathbf{B}}_I$ in SFEM is the average value of $\mathbf{B}_I(\mathbf{x})$ over the real physical element. So in the case the elements are parallelograms, the results of SFEM and FEM will be identical.

Hence, the solution of SFEM has the same properties with that of FEM using reduced integration. The element stiffness matrix will contain spurious zeros energy modes, and the global stiffness matrix after imposing essential boundary conditions can be singular depending on the setting of the problem [13, 14]. \square

5. VARIATIONAL CONSISTENCY OF QUADRILATERAL SFEM ELEMENTS

In this section, we will examine the variational consistency of quadrilateral SFEM elements using a number of SCs and calculating matrix $\tilde{\mathbf{B}}_I$ on each SC.

If we divide domain Ω into a number of quadrilateral SCs Ω_C such that $\Omega = \Omega_1 \cup \Omega_2 \cup \dots \cup \Omega_{SC}$ and $\Omega_1 \cap \Omega_2 \cap \dots \cap \Omega_{SC} = \emptyset$, Equation (35) will have the form

$$\mathbf{K}_{SC-IJ}^{SFEM} = \sum_{C=1}^{SC} \int_{\Omega_C} \tilde{\mathbf{B}}_{CI}^T \mathbf{D} \tilde{\mathbf{B}}_{CJ} d\Omega \quad (40)$$

where

$$\begin{aligned} \tilde{\mathbf{B}}_{CI} &= \int_{\Omega_C} \frac{1}{AC} \mathbf{B}_I(\mathbf{x}) d\Omega = \int_{\Omega_C} \frac{1}{AC} \nabla_S N_I(\mathbf{x}) d\Omega = \int_{\Gamma_C} \frac{1}{AC} N_I(\mathbf{x}) \mathbf{n}_C(\mathbf{x}) d\Gamma \\ &= \begin{bmatrix} \int_{\Gamma_C} \frac{1}{AC} N_I(\mathbf{x}) n_{Cx}(\mathbf{x}) d\Gamma & 0 \\ 0 & \int_{\Gamma_C} \frac{1}{AC} N_I(\mathbf{x}) n_{Cy}(\mathbf{x}) d\Gamma \\ \int_{\Gamma_C} \frac{1}{AC} N_I(\mathbf{x}) n_{Cy}(\mathbf{x}) d\Gamma & \int_{\Gamma_C} \frac{1}{AC} N_I(\mathbf{x}) n_{Cx}(\mathbf{x}) d\Gamma \end{bmatrix} \end{aligned} \quad (41)$$

where $A_C = \int_{\Omega_C} d\Omega$ is the area of smoothed cell Ω_C , Γ_C is the boundary of smoothed cell Ω_C . Note that $\tilde{\mathbf{B}}_{CI}$ depends on the area A_C rather than the area A of $\tilde{\mathbf{B}}_I$.

As proved in Section 4, if $SC = 1$, the calculation of the stiffness matrix $\mathbf{K}_{IJ}^{\text{SFEM}}$ in Equation (35), with $\tilde{\mathbf{B}}_I = \int_{\Omega} \frac{1}{A} \nabla_S N_I(\mathbf{x}) d\Omega$ being the average value of $\nabla N_I(\mathbf{x})$ in the domain Ω , will lead to a solution of whose properties are similar to that of FEM using reduced integration.

Theorem 3

If $SC \rightarrow \infty$ and the domain of the cell $\Omega_C \rightarrow 0$, the stiffness matrix $\mathbf{K}_{SC-IJ}^{\text{SFEM}}$ in Equation (40) will approach the stiffness matrix $\mathbf{K}_{IJ}^{\text{FEM}} = \int_{\Omega} \mathbf{B}_I^T(\mathbf{x}) \mathbf{D} \mathbf{B}_J(\mathbf{x}) d\Omega$ using ‘full’ (2×2) Gauss integration. In this case, the solution of SFEM will approach the standard compatible displacement FEM model.

Proof

$$\begin{aligned} \lim_{SC \rightarrow \infty} \mathbf{K}_{SC-IJ}^{\text{SFEM}} &= \lim_{SC \rightarrow \infty} \sum_{C=1}^{SC} \int_{\Omega_C} \tilde{\mathbf{B}}_{CI}^T \mathbf{D} \tilde{\mathbf{B}}_{CJ} d\Omega = \lim_{SC \rightarrow \infty} \sum_{C=1}^{SC} \tilde{\mathbf{B}}_{CI}^T \mathbf{D} \tilde{\mathbf{B}}_{CJ} A_C \\ &= \lim_{SC \rightarrow \infty} \sum_{C=1}^{SC} \left(\int_{\Omega_C} \mathbf{B}_I(\mathbf{x}) \frac{1}{A_C} d\Omega \right)^T \mathbf{D} \left(\int_{\Omega_C} \mathbf{B}_J(\mathbf{x}) \frac{1}{A_C} d\Omega \right) \cdot A_C \\ &= \lim_{SC \rightarrow \infty} \sum_{C=1}^{SC} \mathbf{B}_I^T(\xi_C) \mathbf{D} \mathbf{B}_J(\xi_C) \cdot A_C = \int_{\Omega} \mathbf{B}_I^T(\mathbf{x}) \mathbf{D} \mathbf{B}_J(\mathbf{x}) d\Omega \\ &= \mathbf{K}_{IJ}^{\text{FEM}} \end{aligned}$$

where ξ_C is a point in Ω_C . □

Note that $\tilde{\mathbf{B}}_{CI}$ and \mathbf{D} are constants in the domain of the cell Ω_C . When $SC \rightarrow \infty$ and Ω_C approaches an infinitesimal area, and because $\mathbf{B}_I(\mathbf{x})$ is continuous, $\int_{\Omega_C} \mathbf{B}_I(\mathbf{x}) \frac{1}{A_C} d\Omega \rightarrow \mathbf{B}_I(\xi_C)$. The above proof can be simply explained as, when the number of $SC \rightarrow \infty$, domain Ω_C will approach an infinitesimal area containing a point ξ_C , the average value of $\mathbf{B}_I(\mathbf{x}) = \nabla N_I(\mathbf{x})$ over a domain Ω_C will approach the value at the converged point ξ_C , $\tilde{\mathbf{B}}_I = \int_{\Omega_C} \mathbf{B}_I(\mathbf{x}) \frac{1}{A_C} d\Omega \rightarrow \mathbf{B}_I(\xi_C)$. In other words, smoothing of any continuous function over points returns the function itself.

Theorem 4

For any finite positive integer of SC larger than 1, the orthogonal condition equation (34) will not be satisfied, and hence SFEM is not ‘variationally consistent’ based on the definition of Equation (34), and the elements of the SFEM will not satisfy both equilibrium and compatibility in the element level.

Proof

Note that the orthogonal condition equation (34) is only satisfied for two cases, $SC = 1$ and $SC \rightarrow \infty$. Suppose that the orthogonal condition equation (34) will be satisfied with any finite

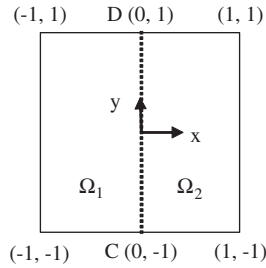


Figure 1. Two smoothing cells with equal area.

number of SC larger than 1, then

$$\begin{aligned}
 \mathbf{K}_{SC-IJ}^{SFEM} &= \mathbf{K}_{IJ}^{SFEM} \\
 &\Leftrightarrow \sum_{C=1}^{SC} \int_{\Omega_C} \tilde{\mathbf{B}}_{CI}^T \mathbf{D} \tilde{\mathbf{B}}_{CJ} \, d\Omega = \int_{\Omega} \tilde{\mathbf{B}}_I^T \mathbf{D} \tilde{\mathbf{B}}_J \, d\Omega \\
 &\Leftrightarrow \sum_{C=1}^{SC} \int_{\Omega_C} \left(\int_{\Omega_C} \frac{\mathbf{B}_I(\mathbf{x})}{A_C} \, d\Omega \right)^T \mathbf{D} \left(\int_{\Omega_C} \frac{\mathbf{B}_J(\mathbf{x})}{A_C} \, d\Omega \right) \, d\Omega = \sum_{C=1}^{SC} \int_{\Omega_C} \tilde{\mathbf{B}}_I^T \mathbf{D} \tilde{\mathbf{B}}_J \, d\Omega \\
 &\Leftrightarrow \sum_{C=1}^{SC} \int_{\Omega_C} \left(\int_{\Omega_C} \frac{\mathbf{B}_I(\mathbf{x})}{A_C} \, d\Omega \right)^T \mathbf{D} \left(\int_{\Omega_C} \frac{\mathbf{B}_J(\mathbf{x})}{A_C} \, d\Omega \right) \, d\Omega \\
 &= \sum_{C=1}^{SC} \int_{\Omega_C} \left(\int_{\Omega} \frac{\mathbf{B}_I(\mathbf{x})}{A} \, d\Omega \right)^T \mathbf{D} \left(\int_{\Omega} \frac{\mathbf{B}_J(\mathbf{x})}{A} \, d\Omega \right) \, d\Omega \tag{42}
 \end{aligned}$$

Equation (42) holds and is independent of the number of SC and sub-domain Ω_C only when the following equation is satisfied:

$$\int_{\Omega_C} \frac{\mathbf{B}_I(\mathbf{x})}{A_C} \, d\Omega = \int_{\Omega} \frac{\mathbf{B}_I(\mathbf{x})}{A} \, d\Omega \quad \text{for any } C \tag{43}$$

However, Equation (43) is only correct in the case of $\mathbf{B}_I(\mathbf{x})$ being constant. This contradicts the hypothesis of the shape function of the bilinear quadrilateral element that $\mathbf{B}_I(\mathbf{x}) = \nabla_S N_I(\mathbf{x})$ is a linear function of co-ordinates. Therefore, the first statement of Theorem 4 stands.

To show explicitly that Equation (43) cannot be satisfied when $\mathbf{B}_I(\mathbf{x}) = \nabla_S N_I(\mathbf{x})$ is a linear function of co-ordinates, we study a rectangular bilinear element that is divided into two equal SCs Ω_1, Ω_2 such that $A_1 = A_2 = A/2 = 2$, as shown in Figure 1. Without losing generality, the bilinear shape function is given by $N_1(x) = \frac{1}{4}(1-x)(1-y)$, and

$$\mathbf{B}_1(\mathbf{x}) = \nabla_S N_1(\mathbf{x}) = \nabla_S \left(\frac{1}{4}(1-x)(1-y) \right) = \frac{1}{4} \begin{bmatrix} y-1 & 0 \\ 0 & x-1 \\ x-1 & y-1 \end{bmatrix}$$

We then have

$$\int_{\Omega} \frac{\mathbf{B}_1(\mathbf{x})}{A} d\Omega = \frac{1}{4} \cdot \frac{1}{4} \begin{bmatrix} \int_{-1}^1 \int_{-1}^1 (y-1) dx dy & 0 \\ 0 & \int_{-1}^1 \int_{-1}^1 (x-1) dx dy \\ \int_{-1}^1 \int_{-1}^1 (x-1) dx dy & \int_{-1}^1 \int_{-1}^1 (y-1) dx dy \end{bmatrix}$$

$$= \frac{1}{16} \begin{bmatrix} -4 & 0 \\ 0 & -4 \\ -4 & -4 \end{bmatrix} = -\frac{1}{8} \begin{bmatrix} 2 & 0 \\ 0 & 2 \\ 2 & 2 \end{bmatrix} \quad (44)$$

$$\int_{\Omega_1} \frac{\mathbf{B}_1(\mathbf{x})}{A_1} d\Omega = \frac{1}{2} \cdot \frac{1}{4} \begin{bmatrix} \int_{-1}^0 \int_{-1}^1 (y-1) dy dx & 0 \\ 0 & \int_{-1}^1 \int_{-1}^0 (x-1) dx dy \\ \int_{-1}^{-1} \int_{-1}^0 (x-1) dx dy & \int_{-1}^0 \int_{-1}^1 (y-1) dy dx \end{bmatrix}$$

$$= -\frac{1}{8} \begin{bmatrix} 2 & 0 \\ 0 & 3 \\ 3 & 2 \end{bmatrix} \quad (45)$$

$$\int_{\Omega_2} \frac{\mathbf{B}_1(\mathbf{x})}{A_2} d\Omega = \frac{1}{2} \cdot \frac{1}{4} \begin{bmatrix} \int_0^1 \int_{-1}^1 (y-1) dy dx & 0 \\ 0 & \int_{-1}^1 \int_0^1 (x-1) dx dy \\ \int_{-1}^1 \int_0^1 (x-1) dx dy & \int_0^1 \int_{-1}^1 (y-1) dy dx \end{bmatrix} = -\frac{1}{8} \begin{bmatrix} 2 & 0 \\ 0 & 1 \\ 1 & 2 \end{bmatrix} \quad (46)$$

It is clear that

$$\int_{\Omega} \frac{\mathbf{B}_1(\mathbf{x})}{A} d\Omega \neq \int_{\Omega_1} \frac{\mathbf{B}_1(\mathbf{x})}{A_1} d\Omega \neq \int_{\Omega_2} \frac{\mathbf{B}_1(\mathbf{x})}{A_2} d\Omega$$

which implies the invalidation of orthogonal condition of Equation (34) and hence the SFEM is not 'variationally consistent' based on the definition of Equation (34).

We need now to show that the element is neither in equilibrium state nor in compatibility state at the element level.

Similar to Equations (45) and (46), which are $\tilde{\mathbf{B}}_{11}$ and $\tilde{\mathbf{B}}_{21}$, we can calculate $\tilde{\mathbf{B}}_{1I}$ and $\tilde{\mathbf{B}}_{2I}$ for $I = 2, 3, 4$ with the bilinear shape functions $N_2(x) = \frac{1}{4}(1+x)(1-y)$, $N_3(x) = \frac{1}{4}(1+x)(1+y)$ and $N_4(x) = \frac{1}{4}(1-x)(1+y)$:

$$\tilde{\mathbf{B}}_{12} = \int_{\Omega_1} \frac{\mathbf{B}_2(\mathbf{x})}{A_1} d\Omega = \frac{1}{8} \begin{bmatrix} 2 & 0 \\ 0 & -1 \\ -1 & 2 \end{bmatrix}, \quad \tilde{\mathbf{B}}_{22} = \int_{\Omega_2} \frac{\mathbf{B}_2(\mathbf{x})}{A_2} d\Omega = \frac{1}{8} \begin{bmatrix} 2 & 0 \\ 0 & -3 \\ -3 & 2 \end{bmatrix} \quad (47)$$

$$\tilde{\mathbf{B}}_{13} = \int_{\Omega_1} \frac{\mathbf{B}_3(\mathbf{x})}{A_1} d\Omega = \frac{1}{8} \begin{bmatrix} 2 & 0 \\ 0 & 1 \\ 1 & 2 \end{bmatrix}, \quad \tilde{\mathbf{B}}_{23} = \int_{\Omega_2} \frac{\mathbf{B}_3(\mathbf{x})}{A_2} d\Omega = \frac{1}{8} \begin{bmatrix} 2 & 0 \\ 0 & 3 \\ 3 & 2 \end{bmatrix} \quad (48)$$

$$\tilde{\mathbf{B}}_{14} = \int_{\Omega_1} \frac{\mathbf{B}_4(\mathbf{x})}{A_1} d\Omega = \frac{1}{8} \begin{bmatrix} -2 & 0 \\ 0 & 3 \\ 3 & -2 \end{bmatrix}, \quad \tilde{\mathbf{B}}_{24} = \int_{\Omega_2} \frac{\mathbf{B}_4(\mathbf{x})}{A_2} d\Omega = \frac{1}{8} \begin{bmatrix} -2 & 0 \\ 0 & 1 \\ 1 & -2 \end{bmatrix} \quad (49)$$

From Equations (25), (45)–(49) we obtain the strains in the two smoothed cells (see Figure 1) as follows:

$$\tilde{\boldsymbol{\varepsilon}}_2^h = \sum_{I=1}^4 \tilde{\mathbf{B}}_{1I} \mathbf{d}_I = \frac{1}{8} \begin{bmatrix} -2 & 0 & 2 & 0 & 2 & 0 & -2 & 0 \\ 0 & -3 & 0 & -1 & 0 & 1 & 0 & 3 \\ -3 & -2 & -1 & 2 & 1 & 2 & 3 & -2 \end{bmatrix} \begin{bmatrix} u_1 \\ v_1 \\ u_2 \\ v_2 \\ u_3 \\ v_3 \\ u_4 \\ v_4 \end{bmatrix} \quad (50)$$

$$\tilde{\boldsymbol{\varepsilon}}_2^h = \sum_{I=1}^4 \tilde{\mathbf{B}}_{2I} \mathbf{d}_I = \frac{1}{8} \begin{bmatrix} -2 & 0 & 2 & 0 & 2 & 0 & -2 & 0 \\ 0 & -1 & 0 & -3 & 0 & 3 & 0 & 1 \\ -1 & -2 & -3 & 2 & 3 & 2 & 1 & -2 \end{bmatrix} \begin{bmatrix} u_1 \\ v_1 \\ u_2 \\ v_2 \\ u_3 \\ v_3 \\ u_4 \\ v_4 \end{bmatrix} \quad (51)$$

From Equations (50), (51), it is easy to see that the strains $\tilde{\boldsymbol{\varepsilon}}_1^h, \tilde{\boldsymbol{\varepsilon}}_2^h$ in the two SCs are different for any non-trivial nodal displacements (zero or rigid movements). This leads to that the stresses $\boldsymbol{\sigma}_1^h = \mathbf{D}\tilde{\boldsymbol{\varepsilon}}_1^h$ and $\boldsymbol{\sigma}_2^h = \mathbf{D}\tilde{\boldsymbol{\varepsilon}}_2^h$ are different and hence stress is discontinuous on the cell interface CD (see Figure 1). Therefore, the quadrilateral bilinear element with two cells does not satisfy equilibrium on the cell interface. According to Lemma 2, the compatibility within the cells is also violated. \square

Note that the above proof is based on SC = 2, but it can be easily extended to any finite number of SC larger than 1 by simple induction.

Theorem 4 naturally gives rise to a question: is the SFEM solution reliable when a finite number of cells are used? The following theorem provides a positive and a very powerful answer.

Theorem 5

Consider an SFEM element that is divided *sequentially*[‡] into $n \geq 1$ SCs. Let the strain energy of an element with SC = i cells be

$$E_{SC=i}^{SFEM} = \sum_{C=1}^i \int_{\Omega_C} \tilde{\boldsymbol{\varepsilon}}_{\Omega_C}^T \mathbf{D} \tilde{\boldsymbol{\varepsilon}}_{\Omega_C} d\Omega = \sum_{C=1}^i \tilde{\boldsymbol{\varepsilon}}_{\Omega_C}^T \mathbf{D} \tilde{\boldsymbol{\varepsilon}}_{\Omega_C} A_{\Omega_C} \tag{52}$$

We then have the following monotonic inequality

$$E_{SC=1}^{SFEM} < E_{SC=2}^{SFEM} < \dots < E_{SC=n-1}^{SFEM} < E_{SC=n}^{SFEM} < E_{SC=n+1}^{SFEM} < \dots < E_{SC \rightarrow \infty}^{SFEM} = E^{FEM} \tag{53}$$

Proof

Suppose that the domain Ω of the quadrilateral element had already divided into n SCs $\Omega_n (n \geq 1)$ such that $\Omega = \Omega_1 \cup \Omega_2 \cup \dots \cup \Omega_n$ and $\Omega_1 \cap \Omega_2 \cap \dots \cap \Omega_n = \emptyset$. Let $E_{SC=n}^{SFEM}$ be the strain energy of the element when SC = n . We now further divide the i th SC Ω_i into two SCs Ω_{i1} and Ω_{i2} such that $\Omega_i = \Omega_{i1} \cup \Omega_{i2}$ and $\Omega_{i1} \cap \Omega_{i2} = \emptyset$, which results in a total of SC = $n + 1$ SCs. Then, the strain energy of the element becomes $E_{SC=n+1}^{SFEM}$. Let $\boldsymbol{\varepsilon}^h$ be the strain vector of the corresponding element of the standard displacement compatible FEM. Then, we have the following relationship for the smoothed strains:

$$\begin{aligned} \tilde{\boldsymbol{\varepsilon}}_{\Omega_i}^h &= \frac{1}{A_{\Omega_i}} \int_{\Omega_i} \boldsymbol{\varepsilon}^h d\Omega = \frac{1}{A_{\Omega_i}} \left[A_{\Omega_{i1}} \int_{\Omega_{i1}} \frac{\boldsymbol{\varepsilon}^h}{A_{\Omega_{i1}}} d\Omega + A_{\Omega_{i2}} \int_{\Omega_{i2}} \frac{\boldsymbol{\varepsilon}^h}{A_{\Omega_{i2}}} d\Omega \right] \\ &= \underbrace{\frac{A_{\Omega_{i1}}}{A_{\Omega_i}}}_{\alpha_1} \tilde{\boldsymbol{\varepsilon}}_{\Omega_{i1}}^h + \underbrace{\frac{A_{\Omega_{i2}}}{A_{\Omega_i}}}_{\alpha_2} \tilde{\boldsymbol{\varepsilon}}_{\Omega_{i2}}^h \\ &= \alpha_1 \tilde{\boldsymbol{\varepsilon}}_{\Omega_{i1}}^h + \alpha_2 \tilde{\boldsymbol{\varepsilon}}_{\Omega_{i2}}^h \end{aligned} \tag{54}$$

where $\tilde{\boldsymbol{\varepsilon}}_{\Omega_i}^h$ is the smoothed strain of domain Ω_i corresponding to SC = n ; $\tilde{\boldsymbol{\varepsilon}}_{\Omega_{i1}}^h$ and $\tilde{\boldsymbol{\varepsilon}}_{\Omega_{i2}}^h$ are the smoothed strains of domains Ω_{i1} and Ω_{i2} corresponding to SC = $n + 1$; A_{Ω_i} is the area of domain

[‡]The division of SC = $n + 1$ is performed by dividing any of the cells in the previous division of SC = n .

Ω_i corresponding to $SC = n$, $A_{\Omega_{i1}}$ and $A_{\Omega_{i2}}$ are the areas of domains Ω_{i1} and Ω_{i2} corresponding to $SC = n + 1$; $\alpha_1 = A_{\Omega_{i1}}/A_{\Omega_i} > 0$ and $\alpha_2 = A_{\Omega_{i2}}/A_{\Omega_i} > 0$. Note that, we have the relationship

$$\alpha_1 + \alpha_2 = 1 \quad (55)$$

Considering the difference between $E_{SC=n+1}^{SFEM}$ and $E_{SC=n}^{SFEM}$, and using Equations (54) and (55), we obtain

$$\begin{aligned} E_{SC=n+1}^{SFEM} - E_{SC=n}^{SFEM} &= (\tilde{\boldsymbol{\varepsilon}}_{\Omega_{i1}}^h)^T \mathbf{D} \tilde{\boldsymbol{\varepsilon}}_{\Omega_{i1}}^h A_{\Omega_{i1}} + (\tilde{\boldsymbol{\varepsilon}}_{\Omega_{i2}}^h)^T \mathbf{D} \tilde{\boldsymbol{\varepsilon}}_{\Omega_{i2}}^h A_{\Omega_{i2}} - (\tilde{\boldsymbol{\varepsilon}}_{\Omega_i}^h)^T \mathbf{D} \tilde{\boldsymbol{\varepsilon}}_{\Omega_i}^h A_{\Omega_i} \\ &= \left((\tilde{\boldsymbol{\varepsilon}}_{\Omega_{i1}}^h)^T \mathbf{D} (\tilde{\boldsymbol{\varepsilon}}_{\Omega_{i1}}^h) \frac{A_{\Omega_{i1}}}{A_{\Omega_i}} + (\tilde{\boldsymbol{\varepsilon}}_{\Omega_{i2}}^h)^T \mathbf{D} (\tilde{\boldsymbol{\varepsilon}}_{\Omega_{i2}}^h) \frac{A_{\Omega_{i2}}}{A_{\Omega_i}} - (\tilde{\boldsymbol{\varepsilon}}_{\Omega_i}^h)^T \mathbf{D} (\tilde{\boldsymbol{\varepsilon}}_{\Omega_i}^h) \right) A_{\Omega_i} \\ &= (\alpha_1 (\tilde{\boldsymbol{\varepsilon}}_{\Omega_{i1}}^h)^T \mathbf{D} \tilde{\boldsymbol{\varepsilon}}_{\Omega_{i1}}^h + \alpha_2 (\tilde{\boldsymbol{\varepsilon}}_{\Omega_{i2}}^h)^T \mathbf{D} \tilde{\boldsymbol{\varepsilon}}_{\Omega_{i2}}^h - (\alpha_1 \tilde{\boldsymbol{\varepsilon}}_{\Omega_{i1}}^h + \alpha_2 \tilde{\boldsymbol{\varepsilon}}_{\Omega_{i2}}^h)^T \mathbf{D} (\alpha_1 \tilde{\boldsymbol{\varepsilon}}_{\Omega_{i1}}^h + \alpha_2 \tilde{\boldsymbol{\varepsilon}}_{\Omega_{i2}}^h)) A_{\Omega_i} \\ &= ((\alpha_1 - \alpha_1^2) (\tilde{\boldsymbol{\varepsilon}}_{\Omega_{i1}}^h)^T \mathbf{D} \tilde{\boldsymbol{\varepsilon}}_{\Omega_{i1}}^h + (\alpha_2 - \alpha_2^2) (\tilde{\boldsymbol{\varepsilon}}_{\Omega_{i2}}^h)^T \mathbf{D} \tilde{\boldsymbol{\varepsilon}}_{\Omega_{i2}}^h \\ &\quad - \alpha_1 \alpha_2 ((\tilde{\boldsymbol{\varepsilon}}_{\Omega_{i1}}^h)^T \mathbf{D} \tilde{\boldsymbol{\varepsilon}}_{\Omega_{i2}}^h + (\tilde{\boldsymbol{\varepsilon}}_{\Omega_{i2}}^h)^T \mathbf{D} \tilde{\boldsymbol{\varepsilon}}_{\Omega_{i1}}^h)) A_{\Omega_i} \\ &= (\alpha_1 (1 - \alpha_1) (\tilde{\boldsymbol{\varepsilon}}_{\Omega_{i1}}^h)^T \mathbf{D} \tilde{\boldsymbol{\varepsilon}}_{\Omega_{i1}}^h + \alpha_2 (1 - \alpha_2) (\tilde{\boldsymbol{\varepsilon}}_{\Omega_{i2}}^h)^T \mathbf{D} \tilde{\boldsymbol{\varepsilon}}_{\Omega_{i2}}^h \\ &\quad - \alpha_1 \alpha_2 ((\tilde{\boldsymbol{\varepsilon}}_{\Omega_{i1}}^h)^T \mathbf{D} \tilde{\boldsymbol{\varepsilon}}_{\Omega_{i2}}^h + (\tilde{\boldsymbol{\varepsilon}}_{\Omega_{i2}}^h)^T \mathbf{D} \tilde{\boldsymbol{\varepsilon}}_{\Omega_{i1}}^h)) A_{\Omega_i} \\ &= ((\tilde{\boldsymbol{\varepsilon}}_{\Omega_{i1}}^h)^T \mathbf{D} \tilde{\boldsymbol{\varepsilon}}_{\Omega_{i1}}^h + (\tilde{\boldsymbol{\varepsilon}}_{\Omega_{i2}}^h)^T \mathbf{D} \tilde{\boldsymbol{\varepsilon}}_{\Omega_{i2}}^h - ((\tilde{\boldsymbol{\varepsilon}}_{\Omega_{i1}}^h)^T \mathbf{D} \tilde{\boldsymbol{\varepsilon}}_{\Omega_{i2}}^h + (\tilde{\boldsymbol{\varepsilon}}_{\Omega_{i2}}^h)^T \mathbf{D} \tilde{\boldsymbol{\varepsilon}}_{\Omega_{i1}}^h)) \alpha_1 \alpha_2 A_{\Omega_i} \\ &= (\tilde{\boldsymbol{\varepsilon}}_{\Omega_{i1}}^h - \tilde{\boldsymbol{\varepsilon}}_{\Omega_{i2}}^h)^T \mathbf{D} (\tilde{\boldsymbol{\varepsilon}}_{\Omega_{i1}}^h - \tilde{\boldsymbol{\varepsilon}}_{\Omega_{i2}}^h) \alpha_1 \alpha_2 A_{\Omega_i} > 0 \end{aligned} \quad (56)$$

where we used the SPD property of \mathbf{D} matrix.

By combining Equation (56) with Theorem 3, we obtain inequality (53). \square

The monotonic inequality (53) is a very powerful and useful statement that resulted from the application of smoothing operations to functions in a positive definite quadratic functional. Theorem 5 also means that with the same displacement \mathbf{u}^h , the strain energy of the element with $SC = n + 1$ cells is larger than that of the element with $SC = n$ cells. Or in other words, the stiffness matrix of the element with $SC = n + 1$ cells is stiffer than that of the element with $SC = n$ cells which gives the following corollary.

Corollary 1

Let $\mathbf{K}_{SC=i}^{SFEM}$ be the stiffness matrix of the element with $SC = i$ cells, we then have

$$\mathbf{K}_{SC=1}^{SFEM} < \mathbf{K}_{SC=2}^{SFEM} < \cdots < \mathbf{K}_{SC=n-1}^{SFEM} < \mathbf{K}_{SC=n}^{SFEM} < \mathbf{K}_{SC=n+1}^{SFEM} < \cdots < \mathbf{K}_{SC \rightarrow \infty}^{SFEM} = \mathbf{K}^{FEM} \quad (57)$$

where symbol $<$ means that the stiffness matrix is *softer*.

Corollary 1 can be explained intuitively as follows: when the number of SC increases, the stiffness matrix $\mathbf{K}_{SC-IJ}^{SFEM}$ in Equation (40) will become stiffer. The solution will transform gradually

monotonously from the solution of SFEM ($SC = 1$) to that of the compatible displacement FEM model ($SC \rightarrow \infty$).

Based on Theorem 5 and Corollary 1, we have naturally the following corollary.

Corollary 2

For the bilinear quadrilateral elements, let the relative displacement error between the exact solution u_i and the numerical solution u_i^{SC} of SFEM be

$$e_d^{SC} = \frac{\sum_{i=1}^{ndof} (u_i - u_i^{SC})}{\sum_{i=1}^{ndof} |u_i|} \quad (58)$$

where $ndof$ is the total number of degrees of freedom (DOFs) in the problem, SC ($SC \geq 1$) is the number of smoothed cells in the quadrilateral element, then we have

$$e_d^{SC=1} > e_d^{SC=2} > \dots > e_d^{SC-1} > e_d^{SC} > e_d^{SC+1} > \dots > e_d^{SC \rightarrow \infty} = e_d^{FEM} \quad (59)$$

where e_d^{FEM} is the relative displacement error between the exact solution u_i and the numerical solution u_i^{FEM} of FEM.

Theorem 5 states that even when SFEM is not ‘variationally consistent’ by the definition of Equation (34), it produces perfect results that are energy consistent and can have powerful bound properties given in Equations (53), (57) and (59). This can be further explained as follows.

When multiple SCs are used in an element, we observe a unique ‘complementary’ situation: the equilibrium is ensured in each cell because of the equilibrator, but the compatibility is destroyed in the cell. On the cell interfaces, however, the equilibrium (stress continuity) is not guaranteed, but the displacement continuity is ensured due to the use of the same shape functions on the common interfaces of the cells. It is this unique complementary satisfaction of *equilibrium* or *compatibility* conditions in different parts of the element domain and cell interfaces that ensures no energy loss in any of the violation of equilibrium or compatibility conditions, the principle of virtual work is still satisfied, and hence allows the SFEM to produce a solution of some kind of ‘combined’ form of energy principles. We therefore state that the SFEM is *energy consistent*. It is this *complementary theory* that well explains the essence of the SFEM.

6. NUMERICAL RESULTS

In this section, some numerical examples will be analysed using SFEM. However, we will focus on the conformation of the properties of SFEM from our theoretical studies.

6.1. Cantilever beam

A cantilever beam with length L and height D is studied as a benchmark problem here, which is subjected to a parabolic traction at the free end as shown in Figure 2. The beam is assumed to have a unit thickness so that plane stress condition is valid. The analytical solution is available

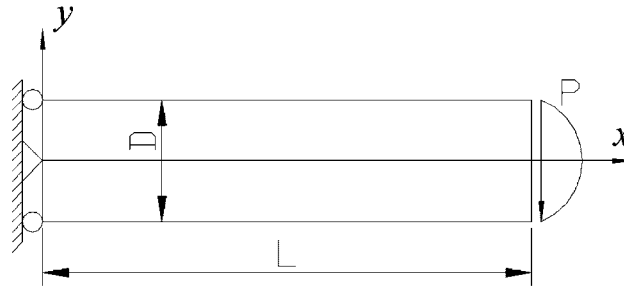


Figure 2. Cantilever beam.

and can be found in a textbook by Timoshenko and Goodier [15].

$$\begin{aligned}
 u_x &= \frac{Py}{6EI} \left[(6L - 3x)x + (2 + \nu) \left(y^2 - \frac{D^2}{4} \right) \right] \\
 u_y &= -\frac{P}{6EI} \left[3\nu y^2(L - x) + (4 + 5\nu) \frac{D^2 x}{4} + (3L - x)x^2 \right]
 \end{aligned} \tag{60}$$

where the moment of inertia I for a beam with rectangular cross section and unit thickness is given by $I = D^3/12$.

The stresses corresponding to the displacement equation (60) are

$$\begin{aligned}
 \sigma_{xx}(x, y) &= \frac{P(L - x)y}{I} \\
 \sigma_{yy}(x, y) &= 0 \\
 \tau_{xy}(x, y) &= -\frac{P}{2I} \left(\frac{D^2}{4} - y^2 \right)
 \end{aligned} \tag{61}$$

The related parameters are taken as $E = 3.0 \times 10^7$ kPa, $\nu = 0.3$, $D = 12$ m, $L = 48$ m and $P = 1000$ N.

Two types of discretization are used (as shown in Figure 3), one with regular elements and the other with irregular interior nodes whose co-ordinates are generated in the following fashion:

$$\begin{aligned}
 x' &= x + \Delta x \cdot r_c \cdot \alpha_{ir} \\
 y' &= y + \Delta y \cdot r_c \cdot \alpha_{ir}
 \end{aligned} \tag{62}$$

where Δx and Δy are initial regular element sizes in x - and y -direction, respectively. r_c is a computer-generated random number between -1.0 and 1.0 and α_{ir} is a prescribed irregularity factor whose value is chosen between 0.0 and 0.5 . The bigger the value of α_{ir} , the more irregular the shape of generated elements.

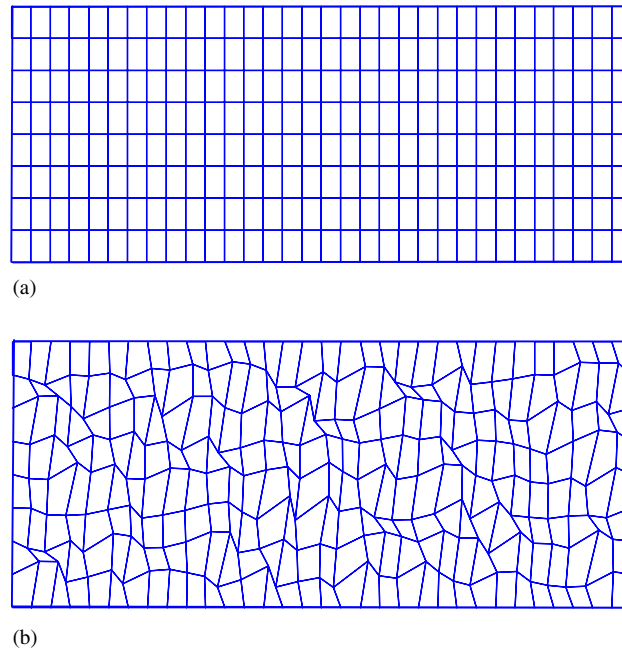


Figure 3. Domain discretization of a beam using 4-node elements: (a) regular elements; and (b) extremely distorted elements.

In order to study the convergence rate of the present method, two norms are used here, i.e. displacement norm and energy norm. The displacement norm is given by

$$e_d = \frac{\sum_{i=1}^{\text{ndof}} |u_i - u_i^h|}{\sum_{i=1}^{\text{ndof}} |u_i|} \quad (63)$$

where u_i is the exact solution and u_i^h is the numerical solution. The following definition is also used:

$$e_{\text{sign}} = \text{sign} \left(\sum_{i=1}^{\text{ndof}} (|u_i^h| - |u_i|) \right) \quad (64)$$

to consider the direction from which side the numerical displacements converge to the exact solution. If $e_{\text{sign}} = 1$, the displacement norm of the numerical solutions will converge to exact solution from upper, on the contrary, if $e_{\text{sign}} = -1$ it will converge to exact solution from lower.

The energy norm is defined by

$$e_c = \frac{1}{2LD} \left[\int_{\Omega} (\boldsymbol{\varepsilon}^h - \boldsymbol{\varepsilon})^T \mathbf{D} (\boldsymbol{\varepsilon}^h - \boldsymbol{\varepsilon}) \right]^{1/2} \quad (65)$$

In the computations, the nodes on the left boundary are constrained using the exact displacements obtained from Equation (60) and the loading on the right boundary uses the distributed parabolic

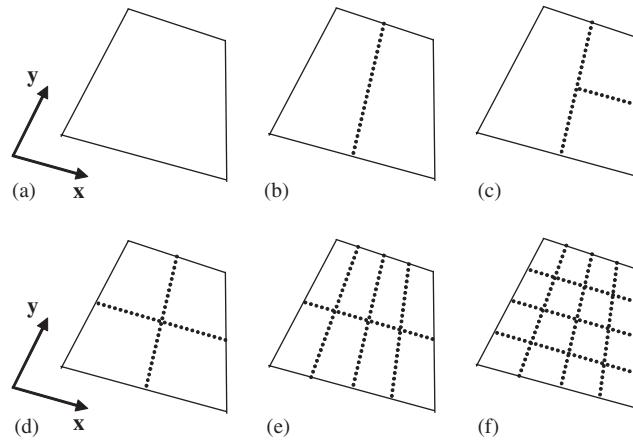


Figure 4. Division of element into the smoothing cells (SC): (a) SC = 1; (b) SC = 2; (c) SC = 3; (d) SC = 4; (e) SC = 8; and (f) SC = 16.

Table I. Tip displacements ($\times 10^{-3}$) of the cantilever beam using different regular elements.

SC	Mesh 16×4	Mesh 32×8	Mesh 64×16	Mesh 128×32
1	9.4542	9.0319	8.9326	8.9081
2	9.2915	8.9948	8.9235	8.9059
3	9.0574	8.9389	8.9097	8.9024
4	8.8355	8.8837	8.8959	8.8990
8	8.7978	8.8741	8.8935	8.8984
16	8.6920	8.8469	8.8866	8.8967
FEM (GP = 4)	8.6453	8.8347	8.8836	8.8959

Note: Analytical solution = 8.900×10^{-3} .

shear stresses in Equation (61). The beam is analysed using different number of elements and smoothing cells, SC = 1, 2, 3, 4, 8 and 16, as shown in Figure 4.

Table I presents the displacement of the middle tip node and Figure 5 shows the relative error in displacement v between SFEM and analytical solution (at $y = 0$, mesh 32×8) of the cantilever using regular elements. From the results in Table I and Figure 5, it is seen that the results of SFEM (SC = 1) and FEM using reduced integration are identical. This is because the elements are rectangular due to regular mesh. It is also seen that when the number of SC of an element increases from 1 to 16, the displacement will change gradually from overestimated to underestimated and approach the result of FEM using 4 Gauss points for full integration. It is observed that an optimal value SC = 4 gives the best results as compared to the exact ones. From this point, we can draw the following remark.

Remark 1

In the case that the solution of SFEM (SC = 1) is overestimated to the exact solution, there exists one optimal value $SC > 1$ (in this example, SC = 4) giving the best results as compared to the exact ones.

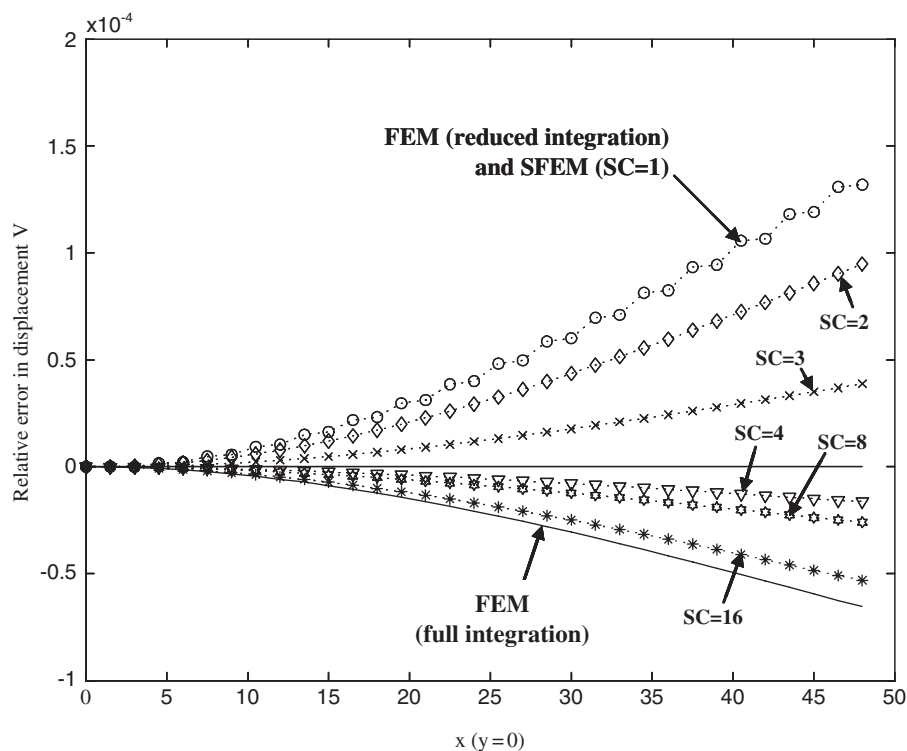


Figure 5. Comparison of the relative error in displacement v between SFEM and analytical solution for the cantilever beam. The monotonic behaviour of the SFEM solution in displacement is clearly shown.

Table II. Displacement error norm of the cantilever beam using different element sizes (regular mesh).

Mesh	Δh	SFEM (SC = 1)	SFEM (SC = 2)	SFEM (SC = 3)	SFEM (SC = 4)	SFEM (SC = 8)	SFEM (SC = 16)	FEM (GP = 4)
16×4	3.0	6.11E-02	4.19E-02	1.66E-02	(-)7.44E-03	(-)1.15E-02	(-)2.29E-02	(-)2.79E-02
32×8	1.5	1.45E-02	1.02E-02	4.10E-03	(-)1.89E-03	(-)2.93E-03	(-)5.88E-03	(-)7.20E-03
64×16	0.75	3.58E-03	2.52E-03	1.02E-03	(-)4.73E-04	(-)7.35E-04	(-)1.48E-03	(-)1.82E-03
128×64	0.375	8.93E-04	6.30E-04	2.56E-04	(-)1.19E-04	(-)1.84E-04	(-)3.71E-04	(-)4.55E-04

Note: sign (-) shows that the solution is smaller than the exact solution; GP = 4 for FEM quadrilateral element is the minimum number for full integration.

The displacement and energy error norms of SFEM are compared with those of 4-node bilinear finite elements in Tables II and III. The convergence rates are also demonstrated in Figure 6(a) and (b). From these results, it is seen that both error norm and convergence rate of SFEM in displacement and energy will approach those of FEM when the number of SC increases.

Table III. Energy error norm of the cantilever beam using different element sizes (regular mesh).

Mesh	Δh	SFEM (SC = 1)	SFEM (SC = 2)	SFEM (SC = 3)	SFEM (SC = 4)	SFEM (SC = 8)	SFEM (SC = 16)	FEM (GP = 4)
16 × 4	3.0	1.68E-04	3.81E-04	3.80E-04	3.97E-04	4.32E-04	4.41E-04	4.55E-04
32 × 8	1.5	4.13E-05	1.78E-04	1.88E-04	2.00E-04	2.18E-04	2.23E-04	2.30E-04
64 × 16	0.75	1.03E-05	8.75E-05	9.37E-05	1.00E-04	1.09E-04	1.12E-04	1.16E-04
128 × 64	0.375	2.59E-06	4.36E-05	4.68E-05	5.01E-05	5.46E-05	5.60E-05	5.78E-05

The results also show that convergence rates in displacement of both methods are roughly equivalent and approximate 2, but the convergence rate of SFEM is slightly larger than that of FEM. The error in energy norm for the SFEM is always smaller than that of FEM, as shown in Figure 6(b). Convergence rate in energy of SFEM when SC = 1 is approximately 2, while those of other SCs are approximately 1. It is also shown that the convergence rate for SFEM of SC > 1 is larger than that of FEM.

To investigate the effect of the shape of quadrilateral element, we perform the same analysis using severely distorted elements created using irregular nodes to compute the error in both displacement and energy. The degree of nodal irregularity α_{ir} is chosen between 0.0 (regular mesh) and 0.4. From Table IV and Figure 7, it is noted that when the mesh becomes more distorted, the displacement error norm of all SCs (except SC = 1) will move closer toward the side of compatible model of FEM. Hence, the displacement error of SC = 2, 3 at some α_{ir} will become even smaller than those of $\alpha_{ir} = 0$ (regular mesh) as they approach and pass across zero error (the exact solution). With the increase of α_{ir} , the displacement errors of SC = 4, 8, 16 and FEM increase. This property shows that all cases of SCs (except SC = 1) have some similarities, for example, the nearly compatible property of displacement.

Table V and Figure 8 show that when the mesh becomes more distorted, the energy error norm of all cases of SCs (SFEM) and FEM increases regularly. These results suggest that if the concerned value of the solution is stress or strain (energy), we should use a regular or less distorted mesh and the optimal value of SC is 4. If the displacement is of concern, we can use a more distorted mesh and the optimal value of SC may be 3. It seems for this problem that an element with non-symmetric SCs, e.g. SC = 3, is the best for a severely distorted mesh, while an element with symmetric SCs, e.g. SC = 4, is the best for a regular or less distorted mesh. Note that when the shape of element is severely distorted ($\alpha_{ir} > 0.2$), FEM may fail to work due to the negative determinant of Jacobian matrix, but the SFEM still works well even when $\alpha_{ir} > 0.4$.

We note that this numerical example confirms the bound properties of SFEM.

6.2. Infinite plate with a circular hole

Figure 9 represents a plate with a central circular hole, radius $a = 1$ m, subjected to a unidirectional tensile load of 1.0 N/m at infinity in the x -direction and Figure 10 gives the discretization of the domain using 4-node elements. Due to its symmetric, only the upper right quadrant of the plate is modelled. Plane strain condition is considered and $E = 1.0 \times 10^3$ N/m², $\nu = 0.3$. Symmetric conditions are imposed on the left and bottom edges, and the inner boundary of the hole is traction

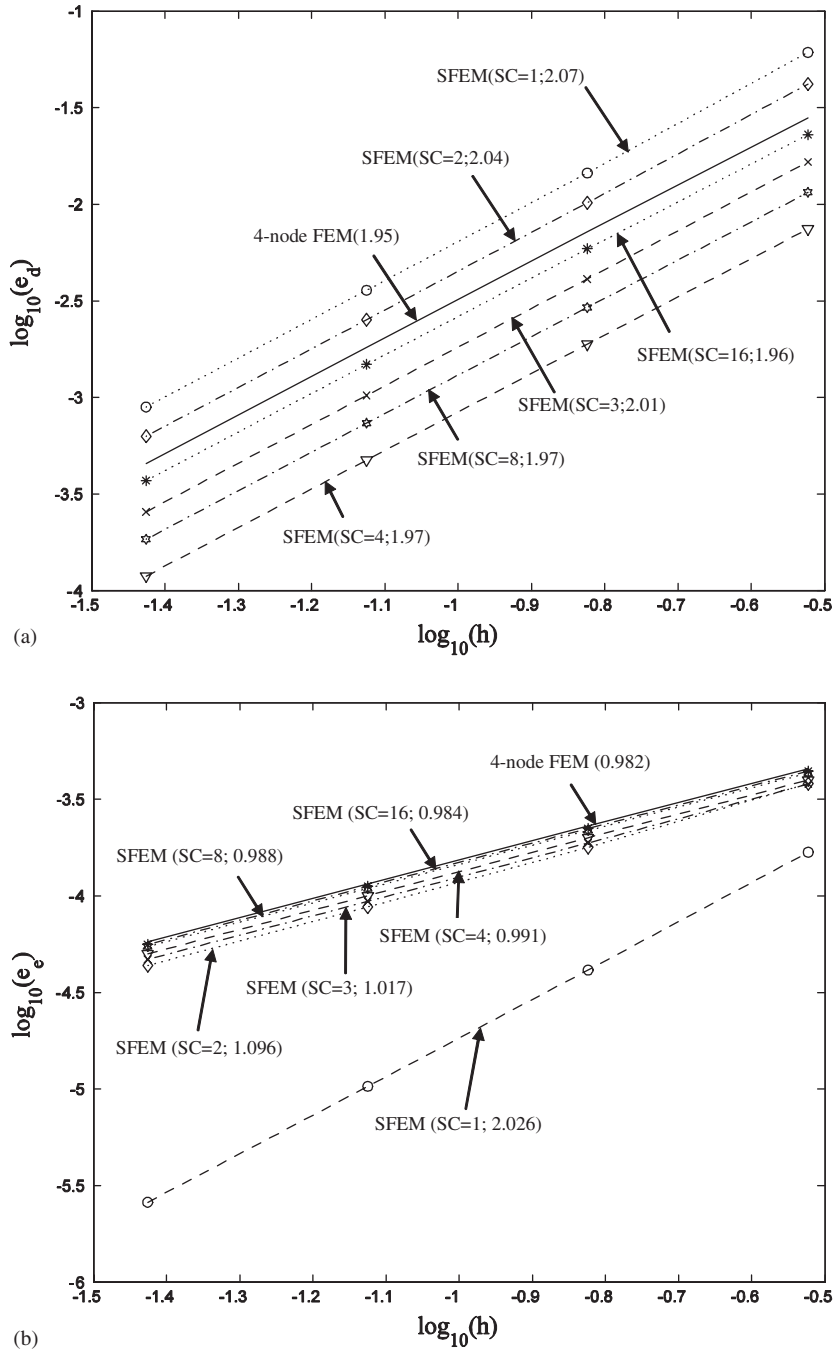


Figure 6. Comparison of convergence rate between SFEM and FEM: (a) displacement norm; and (b) energy norm; the monotonic behaviour of the SFEM solution in energy norm is clearly shown.

Table IV. Displacement error norm of the cantilever beam using irregular elements (mesh 32×8).

α_{ir}	SFEM (SC=1)	SFEM (SC=2)	SFEM (SC=3)	SFEM (SC=4)	SFEM (SC=8)	SFEM (SC=16)	FEM (GP=4)
0.0 (Regular)	1.45E-02	1.02E-02	4.10E-03	(-)1.89E-03	(-)2.93E-03	(-)5.88E-03	(-)7.20E-03
0.1	1.47E-02	1.01E-02	3.86E-03	(-)2.29E-03	(-)3.33E-03	(-)6.31E-03	(-)7.63E-03
0.2	1.89E-02	9.46E-03	3.02E-03	(-)3.29E-03	(-)4.43E-03	(-)7.46E-03	(-)8.81E-03
0.3	1.98E-02	8.23E-03	1.38E-03	(-)5.51E-03	(-)6.76E-03	(-)9.88E-03	Fail
0.4	2.53E-02	7.46E-03	(-)2.06E-03	(-)8.14E-03	(-)9.49E-03	(-)1.28E-02	Fail

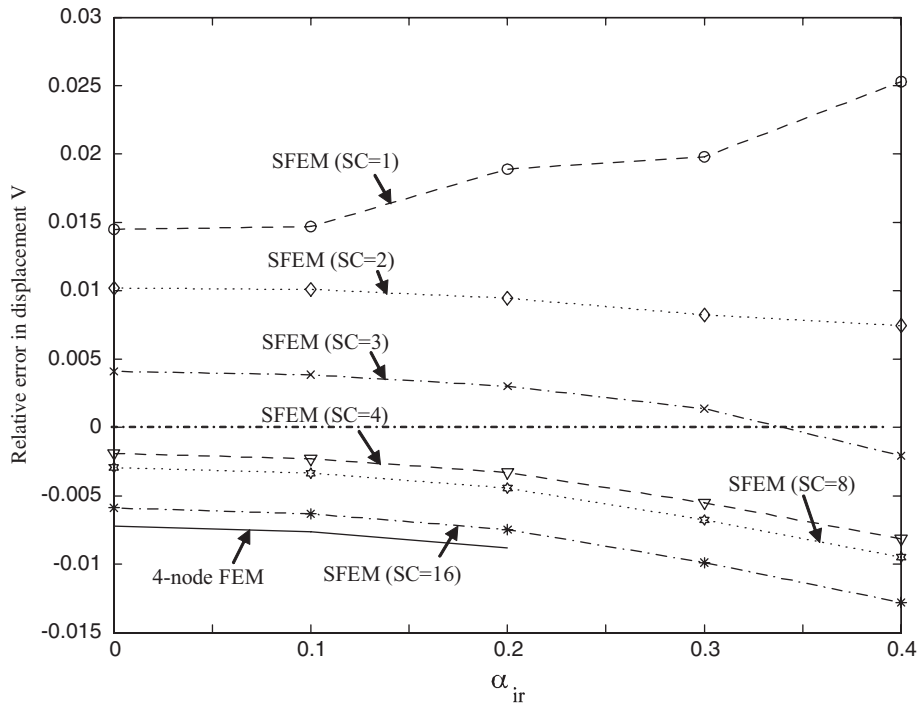


Figure 7. Displacement error norm of the cantilever beam using irregular elements (mesh 32×8).

Table V. Energy error norm of the cantilever beam using irregular elements (mesh 32×8).

α_{ir}	SFEM (SC=1)	SFEM (SC=2)	SFEM (SC=3)	SFEM (SC=4)	SFEM (SC=8)	SFEM (SC=16)	FEM (GP=4)
0.0							
(Regular)	4.13E-05	1.78E-04	1.88E-04	2.00E-04	2.18E-04	2.23E-04	2.30E-04
0.1	5.76E-05	1.86E-04	1.94E-04	2.06E-04	2.24E-04	2.29E-04	2.37E-04
0.2	8.73E-05	2.04E-04	2.12E-04	2.23E-04	2.42E-04	2.48E-04	2.56E-04
0.3	1.28E-04	2.37E-04	2.43E-04	2.55E-04	2.76E-04	2.83E-04	Fail
0.4	1.59E-04	2.77E-04	2.80E-04	2.92E-04	3.15E-04	3.39E-04	Fail

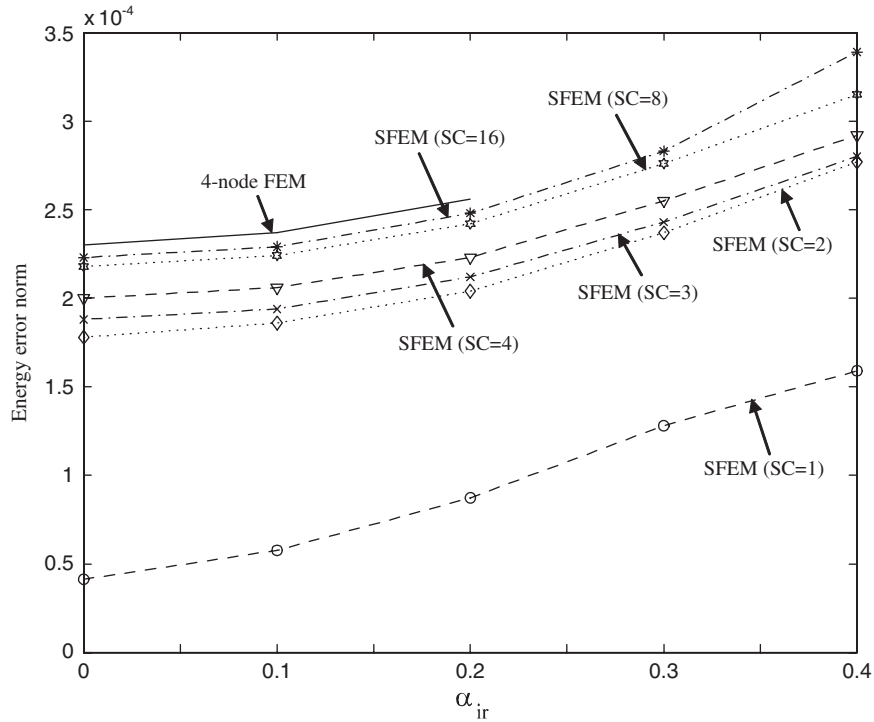


Figure 8. Energy error norm of the cantilever beam using irregular elements (mesh 32×8).

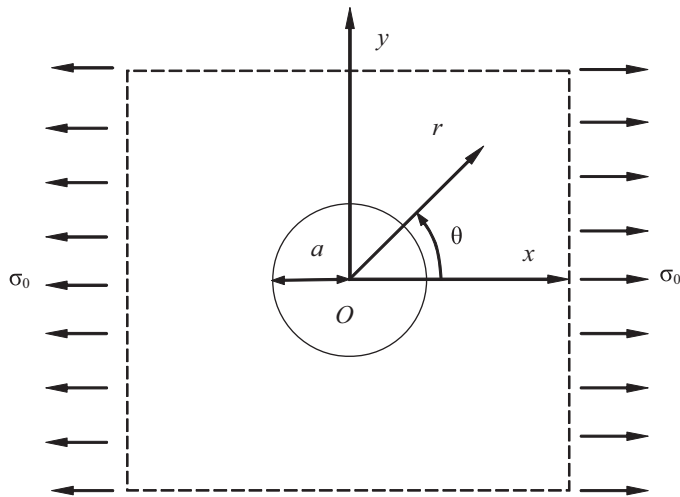


Figure 9. Infinite plate with a circular hole subjected to unidirectional tension.

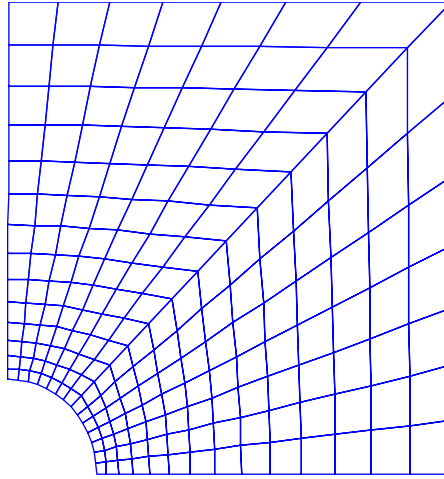


Figure 10. Domain discretization of the infinite plate with a circular hole using 4-node element.

free. The exact solution for the stress [15] is

$$\begin{aligned}\sigma_{11} &= 1 - \frac{a^2}{r^2} \left[\frac{3}{2} \cos 2\theta + \cos 4\theta \right] + \frac{3a^4}{2r^4} \cos 4\theta \\ \sigma_{22} &= -\frac{a^2}{r^2} \left[\frac{1}{2} \cos 2\theta - \cos 4\theta \right] - \frac{3a^4}{2r^4} \cos 4\theta \\ \tau_{12} &= -\frac{a^2}{r^2} \left[\frac{1}{2} \sin 2\theta + \sin 4\theta \right] + \frac{3a^4}{2r^4} \sin 4\theta\end{aligned}\quad (66)$$

where (r, θ) are the polar co-ordinates and θ is measured counterclockwise from the positive x -axis. Traction boundary conditions are imposed on the right ($x = 5$) and top ($y = 5$) edges based on the exact solution equation (66). The displacement components corresponding to the stresses are

$$\begin{aligned}u_1 &= \frac{a}{8\mu} \left[\frac{r}{a} (\kappa + 1) \cos \theta + 2\frac{a}{r} ((1 + \kappa) \cos \theta + \cos 3\theta) - 2\frac{a^3}{r^3} \cos 3\theta \right] \\ u_2 &= \frac{a}{8\mu} \left[\frac{r}{a} (\kappa - 1) \sin \theta + 2\frac{a}{r} ((1 - \kappa) \sin \theta + \sin 3\theta) - 2\frac{a^3}{r^3} \sin 3\theta \right]\end{aligned}\quad (67)$$

where $\mu = E/(2(1 + \nu))$, κ is defined in terms of Poisson ratio by $\kappa = 3 - 4\nu$ for plane strain cases.

The domain is discretized using regular quadrilateral elements divided into different SCs, SC = 1, 2, 4, 8 and 16, as shown in Figure 4. The convergence rates in displacement and energy are demonstrated in Figure 11(a) and (b). Similar to the cantilever beam problem, it is observed that both error norms of SFEM will approach those of FEM when the number of SC increases. The errors in displacement and energy of SFEM are always smaller than those of FEM, and they generally converge in a comparable rate as compared with FEM except SC = 1, for which case the convergence rate is much higher.

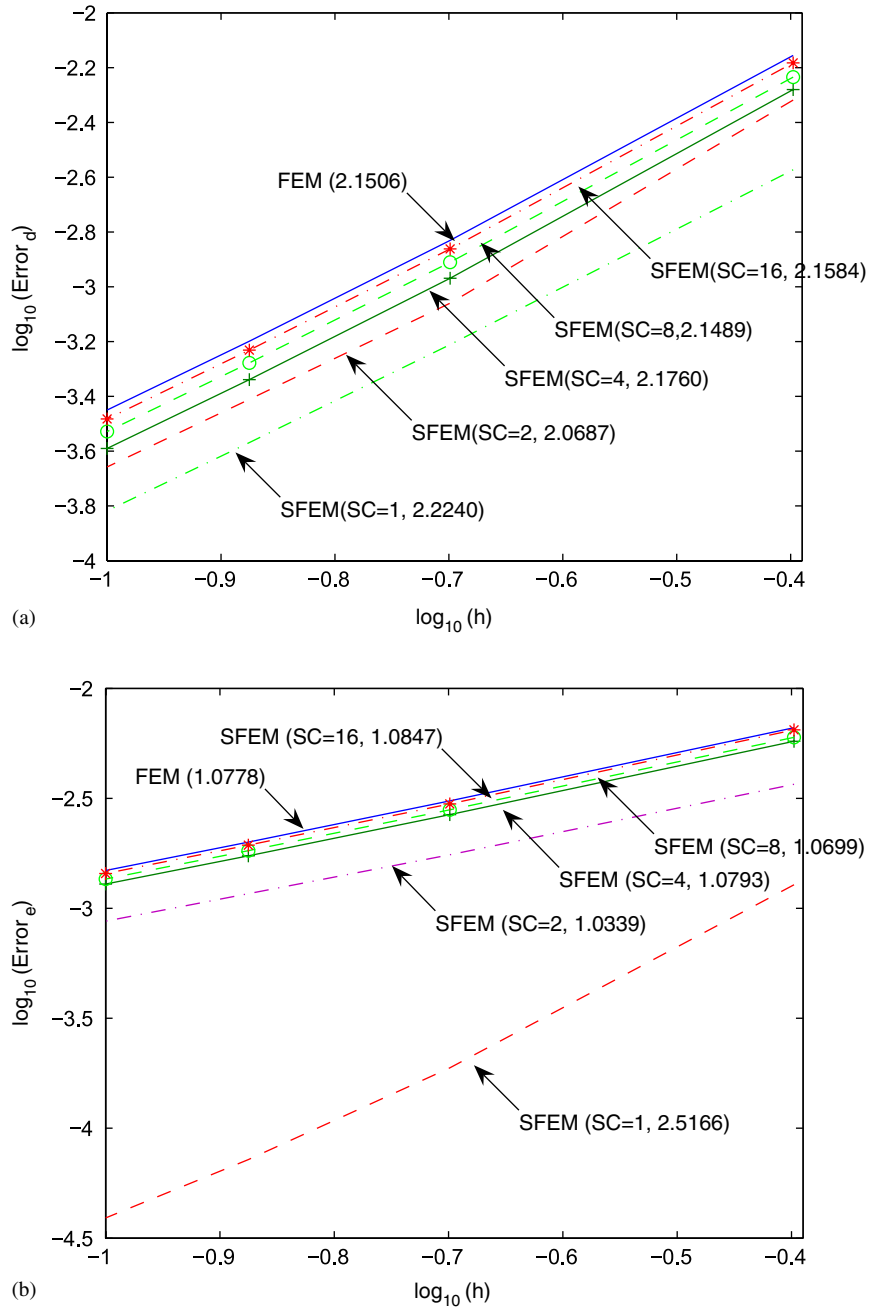


Figure 11. Comparison of convergence rate between SFEM and FEM: (a) displacement norm; and (b) energy norm.

The bound property of SFEM is again strictly observed from this example. Note that from Figure 11(a), the displacement norm of SFEM ($SC = 1$) is the smallest and this norm increases monotonously with the increase of SC. This shows that the solution for all SCs is always underestimated to the exact solution. Hence, we can draw the following remark.

Remark 2

In the case that the solution of SFEM ($SC = 1$) is underestimated to the exact solution, we suggest to use $SC = 2$ to obtain the solution. This solution will be stable (without zeros energy modes) and have the smallest displacement and energy norms.

7. CONCLUSION

In this work, the theoretical bases for SFEM are examined and established in a systematical manner. Through the analytical formulations and numerical examples, some conclusions can be drawn as follows:

1. The Galerkin weak form for SFEM can be established based on Hu–Washizu variational principle or on the mixed variational principle of the assumed strain method, proposed by Simo and Hughes [3].
2. For elastic problems, 1D linear element and 2D linear triangle element of SFEM are identical to their counterparts of FEM. For the quadrilateral element, when the number of SCs of an element of SFEM approaches infinity or equals 1, the solution will be variationally consistent. For any other finite number of SC larger than 1, the solution will not be variationally consistent.
3. For the quadrilateral elements, when the number of SC equals 1, the solution of SFEM has the same properties with those of FEM using reduced integration. The element stiffness matrix will contain spurious zeros energy modes, and the global stiffness matrix after imposing essential boundary conditions can be singular depending on the setting of the problem. When the number of SC approaches infinity, the solution of SFEM will approach the solution of standard displacement compatible FEM model. When the number of SC is a finite number larger than 1, the solutions of SFEM will change monotonously from the solution of SFEM ($SC = 1$) to that of FEM using full integration.
4. In the case that the solution of SFEM ($SC = 1$) is overestimated to the exact solution, there exists one optimal value $SC > 1$ (normally $SC = 4$) which gives the best results as compared to the exact ones. In the case that the solution of SFEM ($SC = 1$) is underestimated to the exact solution, it is suggested that we should use $SC = 2$ to obtain the solution. This solution will be stable (without zeros energy modes) and have the smallest displacement and energy norms. In practical calculation, we can use $SC = 4$ for all problems, the results will be always better than that of standard FEM, and in many cases (not all) this solution is closest to the exact solution.
5. The convergence rates for SFEM in both displacement and energy norms are higher than that for FEM. The error in energy norm is generally smaller than that of FEM. Both error norm and convergence rate of SFEM of both displacement and energy will approach those of FEM when the number of SC increases.
6. SFEM works well even for extremely distorted elements.

Though only 2D elastic problems are considered in this work, there is no technical difficulty in extending the applications of SFEM to other relatively complicated problems, such as 3D problems, geometric and elasto-plastic non-linear problems, higher order elements, etc. Although, more intensive studies need to be conducted in the future, our study so far has convinced that SFEM codes can be developed with minor modifications from the standard existing FEM codes, and they can be widely applied in solving many practical problems for more accurate solutions.

REFERENCES

1. Veubeke BF. Displacement and equilibrium models in the finite element method. In *Stress Analysis*, Zienkiewicz OC, Holister GS (eds). Wiley: London, 1965.
2. Brezzi F, Fortin M. *Mixed and Hybrid Finite Element Methods*. Springer: New York, 1991.
3. Simo JC, Hughes TJR. On the variational foundations of assumed strain methods. *Journal of Applied Mechanics* 1986; **53**:51–54.
4. Simo JC, Hughes TJR. *Computational Inelasticity*. Springer: New York, 1998.
5. Chen JS, Wu CT, Yoon S, You Y. A stabilized conforming nodal integration for Galerkin meshfree method. *International Journal for Numerical Methods in Engineering* 2000; **50**:435–466.
6. Yoo JW, Moran B, Chen JS. Stabilized conforming nodal integration in the natural-element method. *International Journal for Numerical Methods in Engineering* 2004; **60**:861–890.
7. Liu GR, Li Y, Dai KY, Luan MT, Xue W. A linearly conforming RPIM for 2D solid mechanics. *International Journal of Computational Methods* 2006, in press.
8. Bathe KJ. *Finite Element Procedures*. MIT Press/Prentice-Hall: Cambridge, MA, Englewood Cliffs, NJ, 1996.
9. Liu GR, Quek SS. *The Finite Element Method: A Practical Course*. Butterworth Heinemann: Oxford, 2003.
10. Zienkiewicz OC, Taylor RL. *The Finite Element Method* (5th edn). Butterworth Heinemann: Oxford, 2000.
11. Liu GR, Dai KY, Nguyen TT. A smoothed finite element method for mechanics problems. *Computational Mechanics* 2006. Published on line on 17 May 2006, in press.
12. Pian THH, Wu CC. *Hybrid and Incompatible Finite Element Methods*. CRC Press: Boca Raton, FL, 2006.
13. Kelly DW. Reduced integration to give equilibrium models for assessing the accuracy of finite element analysis. *Proceedings of the Third International Conference in Australia on Finite Element Methods*, July 1979.
14. Kelly DW. Bounds on discretization error by special reduced integration of the Lagrange family of finite elements. *International Journal for Numerical Methods in Engineering* 1980; **15**:1489–1506.
15. Timoshenko SP, Goodier JN. *Theory of Elasticity* (3rd edn). McGraw-Hill: New York, 1970.